Progress In Electromagnetics Research, Vol. 117, 19–33, 2011

ITERATIVE TIME-REVERSAL MIRROR METHOD FOR IMAGING THE BURIED OBJECT BENEATH ROUGH GROUND SURFACE

X. Zhu[1], Z. Zhao[1, *], W. Yang[1], Y. Zhang[1], Z. Nie[1], and Q.-H. Liu[2]

[1]School of Electronic Engineering, University of Electronic Science and Technology of China, Chengdu, Sichuan 611731, China

[2]Department of Electrical and Computer Engineering, Duke University, Durham, NC 27708, USA

Abstract—An iterative Time-Reversal Mirror (TRM) method is proposed to Detect and Image the buried target beneath ground surface. Unlike the conventional TRM methods which treat the information of the ground as clutters and directly delete them, the iterative TRM imaging method proposed in this paper utilizes the information of rough ground surface as a useful knowledge. The new approach is consisted of two TRM procedures. In the first TRM procedure, it aims to image the rough surface where the propagation environment for electromagnetic wave is free space. The second TRM procedure aims to image the buried target. In this step, the information of the rough surface estimated by the first TRM procedure will be treated as newly updated propagation environment. Then conventional TRM is applied to image the buried target. By applying this iterative TRM method, the information of the rough ground can be well considered in the whole TRM procedure. Numerical simulations prove that this method performs significantly better image contrast comparing with the results obtained by using conventional TRM. 4–5 dB improvement on the imaging SNR has been achieved. Furthermore, the target can be located more accurately.

Received 13 April 2011, Accepted 18 May 2011, Scheduled 25 May 2011

* Corresponding author: Zhiqin Zhao (zqzhao@uestc.edu.cn).

1. INTRODUCTION

Buried Object Detection (BOD) is a geophysical approach that uses electromagnetic pulse for high-resolution imaging of target buried under the ground surface. BOD has been extensively used in civil engineering [1, 2] and military applications [3], such as landmine or buried water pipe detection, etc.

In order to achieve high resolution, Ultra-wide Band (UWB) electromagnetic (EM) pulse has usually been adopted as transmission source. The difficulties of BOD are quite obvious. Firstly, the information of the ground and the buried target are mixed together. Secondly, the soil attenuates the target echoes badly and makes the situation even worse [4]. In the traditional signal processing methods [5–10], the information of the ground surface is treated as clutters or noise to be canceled, for example, the optimal time-domain detection [5], the iterative frequency-domain clutter reduction [6], hidden Markov models for target classification [7], the ultrawide-band synthetic aperture radar (SAR) processing [8, 9] and traditional Back Projection (BP) method [10], etc. All signal processing idea of these methods is based on data processing, which means they do not put the electromagnetic wave propagation environment into consideration. This limits the resolution and accuracy.

Time reversal mirror (TRM) technique has been convinced to be a rigorous method in imaging and detection of the target in complex environment. The method is based on the principle of reciprocity where the propagation progress of the waves is well considered. Comparing with the traditional technique, TRM has the features of self-averaging and statistical stability properties in the heterogeneous materials [11–13]. The main difference of TRM from the traditional signal processing methods is that TRM utilizes the information of the wave propagation environment. TRM can re-focus the original source or the major scatters both in spatial and time domain simultaneously [14].

The TRM has been widely researched and demonstrated both theoretically and experimentally in acoustic and ultrasonic area [14]. In recent years, TRM has also been proved to be practicable [15, 16] for imaging [17], detection [18, 19] and communication [20] in electromagnetic area. Nevertheless the TRM imaging quality vastly depends on the correctness of modeling the environment [21]. Most previous researches of TRM for BOD are based on the assumption of flat ground or exactly given ground surface [22, 23]. But in real application, one may only have the statistic property of the ground. If we put a random rough surface which satisfies the statistic characteristics in the TRM solving engine, the performance of TRM

will be greatly degraded. If the rough surface can be well acquired and taken account into the TRM process, the imaging quality of the TRM will be significantly improved.

As mentioned before, the TRM imaging quality is affected by the correctness of propagation environment. The environment, such as ground surface or concrete walls, et al., also participates the scattering of the EM pulse, which means that the information induced by the environment will be indeed contained in the echoes. How to extract the information and use it to improve the imaging quality is very important for target detection in complicated environment. Aiming to solve the problem of imaging the buried object beneath rough ground surface, this paper proposes an iterative TRM method. Unlike the conventional TRM methods for BOD problem, this new method performs twice TRM procedures iteratively. It utilizes the information of rough ground surface as a useful knowledge and uses it to estimate the rough surface in the first TRM procedure. In second TRM procedure, the estimated rough surface will be treated as propagation environment. By using this iterative TRM method, the information of the rough ground can be well considered in the whole TRM procedure. Comparing with the conventional TRM methods under the assumption of a flat ground, this new method achieves much better results on the image quality. The simulation results show the effectiveness of the proposed method. Though this paper uses the imaging for the buried object beneath rough ground surface as an example, the idea can be promoted to other TRM imaging applications when the environment clutters and target echoes are mixed.

The remainder of the paper is organized as follows. In Section 2, the new iterative TRM method is proposed. The Green's function is used to describe and derive the iterative TRM process. Some numerical results are shown in Section 3 to demonstrate the improvement of the new method. Conclusions are drawn in the last section.

2. ITERATIVE TRM IMAGING PROCEDURE

The proposed iterative TRM imaging method can be described in Fig. 1.

It is consisted of two steps. In the first step, a free space environment is assumed. Based on this assumption, TRM operation is performed to obtain the image of the ground surface. By using the peak and edge extraction method, the interface of air-ground can be well acquired. In the second step, the surface undulation obtained in the first step will be set as the environment in the TRM procedure. By running the TRM again under the updated environment, the target

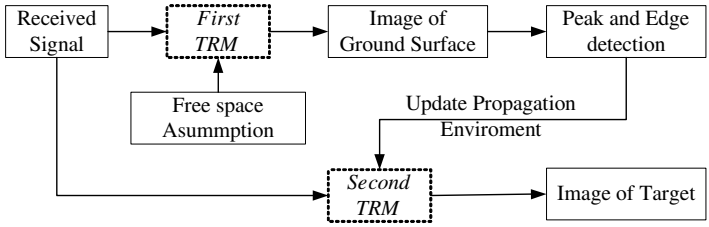

Figure 1. The block scheme of Iterative Time-Reversal Mirror Method.

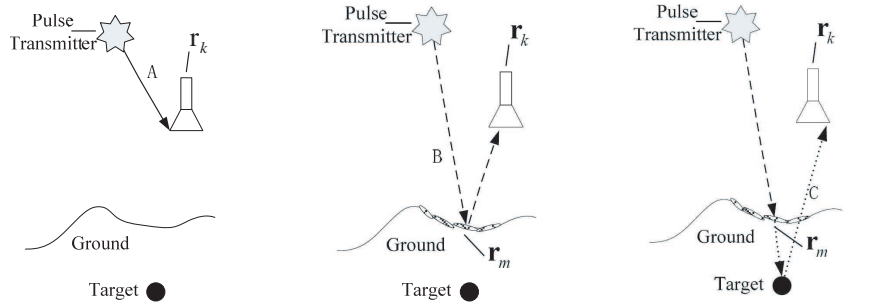

(a) direct signal S_A (b) ground bouncing signal S_B (c) target echo signal S_C

Figure 2. Propagating progress of a typical BOD problem.

echo signal will be refocused so that the target will be imaged beneath the ground.

In order to illustrate this method theoretically, the propagating progress of a UWB pulse is reviewed in Fig. 2. The received signal can be decomposed into three parts.

The first part comes when the UWB pulse directly propagates to the receiver array through the free space, noted as signal S_A shown in Fig. 2(a). Pulse transmitter is placed at position $\mathbf{r}_s$, transmitting an electromagnetic pulse $p(t)$. Suppose the receiver array has K elements $\mathbf{r}_k \,|k \in [1, K]$, the electronic field recorded on the $\mathbf{r}_k$, as signal S_A, is given by,

$$E_{AT}(\mathbf{r}_k, \omega) = \int_{-\infty}^{+\infty} \hat{p}(\omega)\hat{G}_0(\mathbf{r}_k, \mathbf{r}_s, \omega)e^{j\omega t}d\omega \tag{1}$$

where $\hat{p}(\omega)$ is the Fourier transform of the pulse $p(t)$,

$$\hat{p}(\omega) = \int_{-\infty}^{\infty} p(t)e^{-j\omega t}dt \tag{2}$$

and $\hat{G}_0(\mathbf{r}_k, \mathbf{r}, \omega)$ is the Green's function in free space which satisfies the wave equation,

$$\nabla^2 \widehat{G}_0(\mathbf{r}, \mathbf{r}_S, \omega) + \varepsilon_0 \mu_0 \omega^2 \widehat{G}_0(\mathbf{r}, \mathbf{r}_S, \omega) = -\delta(\mathbf{r} - \mathbf{r}_S) \tag{3}$$

The pulse hits the ground surface where it splits into two components: transparent and reflected component. Considering the reflected component first, the ground surface is discretized into several small sections noted as $\mathbf{r}_m \,|m = [1, M]$, and sorted by its distance from $\mathbf{r}_s$

$$|\mathbf{r}_M - \mathbf{r}_s| \geq |\mathbf{r}_{M-1} - \mathbf{r}_s| \geq \cdots \geq |\mathbf{r}_1 - \mathbf{r}_s| \tag{4}$$

The ground surface section $\mathbf{r}_m$ contributes to signal S_B on antenna $\mathbf{r}_k$ is given by

$$\begin{aligned} E_{BTm}(\mathbf{r}_k, \mathbf{r}_m, t) \;=\; & \int_{-\infty}^{+\infty} \underbrace{\hat{p}(\omega)\hat{G}_0(\mathbf{r}_m, \mathbf{r}_s, \omega)}_{\text{forward illuminating}} \\ & \cdot C_m(\omega) \cdot \underbrace{\hat{G}_0(\mathbf{r}_k, \mathbf{r}_m, \omega)}_{\text{backward scattering}} e^{j\omega t} d\omega \end{aligned} \tag{5}$$

Signal S_B indicated in Fig. 2(b) can be summarized as

$$E_{BT}(\mathbf{r}_k, t) = \sum_{m=1}^{M} E_{BTm}(\mathbf{r}_k, \mathbf{r}_m, t) \tag{6}$$

Figure 2(c) stands for the third part of the signal. The transparent component hits the buried target then reflects back through the surface into free space and finally is received by the array. It is noted as signal S_C. In order to simplify the derivation, the reflected component of the ground-air interface is ignored when signal S_C is transmitting from ground to air, i.e., multiple reflections between the target and the ground surface is neglected.

The propagation path of the incident wave from the transmitter to the target and the path of the echo from the target to the receiver antenna $\mathbf{r}_k$ is integrated as two individual Green's functions $\hat{G}_{CI}(\mathbf{r}_t, \mathbf{r}_s, \omega)$ and $\hat{G}_{CR}(\mathbf{r}_t, \mathbf{r}_s, \omega)$. The signal S_C received by antenna $\mathbf{r}_k$ is given by

$$E_{CT}(\mathbf{r}_k, \omega) = \int_{-\infty}^{+\infty} \hat{p}(\omega)\hat{G}_{CI}(\mathbf{r}_t, \mathbf{r}_s, \omega) C_t(\omega) \hat{G}_{CR}(\mathbf{r}_k, \mathbf{r}_t, \omega) e^{j\omega t} d\omega \tag{7}$$

Considering the BOD model is a Linear Time Invariant (LTI) system, the actual signal received by the array is the summation of $E_{AT}(\mathbf{r}_k, t)$, $E_{BT}(\mathbf{r}_k, t)$ and $E_{CT}(\mathbf{r}_k, t)$. $E_{AT}(\mathbf{r}_k, t)$ is easy to be concealed. Because the spatial relation between the transmitter

and the receiver array is well known as the system layout, the $E_{AT}(\mathbf{r}_k, t)$ can be pre-calculated and eliminated as background signal by subtraction [23]. The signal that eventually will be performed by TRM imaging is given by

$$E_R^{\sim}(\mathbf{r}_k, \omega) = \int_{-\infty}^{+\infty} \alpha(\omega)[E_{BT}(\mathbf{r}_k, t) + E_{CT}(\mathbf{r}_k, t)]e^{j\omega t}d\omega \qquad (8)$$

The undulation information of ground surface is certainly in the clutters of ground (signal S_B). If the undulation information can be acquired and injected in building the ground surface, the refocusing performance of TRM for target will be significantly improved. In the forward progress, the pulse hits the ground firstly in a free space, then hits the target secondly in soil. In the reversal progress, if a free space is assumed as background, target echo will be defocused due to the mismatched environment, while the ground scatters will be well focused due to the match background.

$E_R^{\sim}(\mathbf{r}_k, \omega)$ is time reversed in the time domain (conjugated in frequency domain) and re-emitted from antenna element position $\mathbf{r}_k$ respectively. During the propagation, the space-time signal observed in the image domain is

$$I_{1st}(\mathbf{r}, t) = \sum_{k=1}^{K} \int_{-\infty}^{\infty} E_R^{\sim}(\mathbf{r}_k, \omega)^* \hat{G}_{TR}(\mathbf{r}, \mathbf{r}_k, \omega)e^{-j\omega t}d\omega, \qquad (9)$$

where $\hat{G}_{TR}(\mathbf{r}, \mathbf{r}_k, \omega)$ is the calculated Green's function. Generally when perform TRM reversal part, the $\hat{G}_{TR}(\mathbf{r}, \mathbf{r}_k, \omega)$ will be chosen to match the real environment. Now the $E_R^{\sim}(\mathbf{r}_k, \omega)$ contains all the echoes from ground sections and target in soil. Iterative TRM imaging method now is applied as shown in Fig. 3.

Figure 3(a) shows the first TRM environment, where the $\hat{G}_{TR}(\mathbf{r}, \mathbf{r}_k, \omega)$ is basically the Green's function of the free-space. $E_R^{\sim}(\mathbf{r}_k, \omega)^*$ is the time reversed signal sent out from the antenna array.

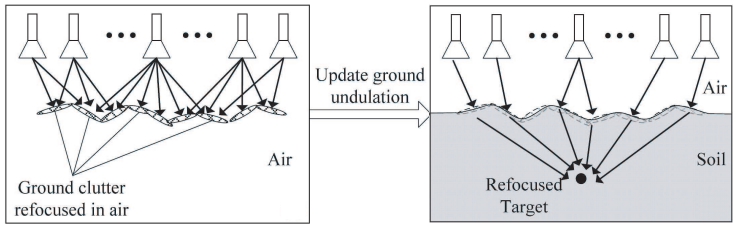

Figure 3. TRM imaging with estimated ground undulation process.

Equation (9) can be derived in frequency domain, (with $\hat{G}_0(\mathbf{r}, \mathbf{r}_k, \omega)$ as $\hat{G}_{TR}(\mathbf{r}, \mathbf{r}_k, \omega)$ in the first iteration)

$$
\begin{aligned}
I_{1st}(\mathbf{r}_m, \omega) &= \delta(\mathbf{r}_m, \mathbf{r}) \cdot I(\mathbf{r}, \omega) = \delta(\mathbf{r}_m, \mathbf{r}) \sum_{k=1}^{K} E_R^{\sim}(\mathbf{r}_k, \omega)^* \hat{G}_0(\mathbf{r}, \mathbf{r}_k, \omega) \\
&= \delta(\mathbf{r}_m, \mathbf{r}) \sum_{k=1}^{K} \left[\sum_{m=1}^{M} E_{BTm}(\mathbf{r}_k, \mathbf{r}_m, t)^* \hat{G}_0(\mathbf{r}, \mathbf{r}_k, \omega) + E_{CT}(\mathbf{r}_k, t)^* \hat{G}_0(\mathbf{r}, \mathbf{r}_k, \omega) \right] \\
&= \delta(\mathbf{r}_m, \mathbf{r}) \sum_{k=1}^{K} \left[\sum_{m=1}^{M} \hat{p}(\omega)^* \hat{G}_0(\mathbf{r}_m, \mathbf{r}_s, \omega)^* \cdot C_m(\omega)^* \cdot \hat{G}_0(\mathbf{r}_k, \mathbf{r}_m, \omega)^* \hat{G}_0(\mathbf{r}, \mathbf{r}_k, \omega) \right. \\
&\quad \left. + \hat{p}(\omega)^* \hat{G}_{CI}(\mathbf{r}_t, \mathbf{r}_s, \omega)^* C_t(\omega)^* \hat{G}_{CR}(\mathbf{r}_k, \mathbf{r}_t, \omega)^* \hat{G}_0(\mathbf{r}, \mathbf{r}_k, \omega) \right] \\
&= \sum_{k=1}^{K} \left[\sum_{m=1}^{M} ILM_B(\mathbf{r}_m, \mathbf{r}_s, \omega) \underbrace{\hat{G}_0(\mathbf{r}_k, \mathbf{r}_m, \omega)^* \hat{G}_0(\mathbf{r}_m, \mathbf{r}_k, \omega)}_{\text{matched and refocused}} \right. \\
&\quad \left. + ILM_C(\mathbf{r}_t, \mathbf{r}_s, \omega) \underbrace{\hat{G}_{CR}(\mathbf{r}_k, \mathbf{r}_t, \omega)^* \hat{G}_0(\mathbf{r}_m, \mathbf{r}_k, \omega)}_{\text{mismatched and defocused}} \right]
\end{aligned} \tag{10}
$$

Because the $\hat{G}_0(\mathbf{r}, \mathbf{r}_k, \omega)$ does not match the actual background of the buried target echo, $E_{CT}(\mathbf{r}_k, t)$ will be defocused. But for $E_{BT}(\mathbf{r}_k, t)$, the clutters of ground sections $\mathbf{r}_m \,|m = [1, M]$, $\hat{G}_0(\mathbf{r}, \mathbf{r}_k, \omega)$ matches the background. They will be refocused chronologically in time-domain, $\mathbf{r}_M$ at first and $\mathbf{r}_1$ at last, as shown in Fig. 3(a).

$$
\begin{aligned}
I_{2nd}(\mathbf{r}_t, \omega) &= \delta(\mathbf{r}_t, \mathbf{r}) \cdot I(\mathbf{r}, \omega) = \delta(\mathbf{r}_t, \mathbf{r}) \sum_{k=1}^{K} E_R^{\sim}(\mathbf{r}_k, \omega)^* \hat{G}_{CR}^{\sim}(\mathbf{r}, \mathbf{r}_k, \omega) \\
&= \sum_{k=1}^{K} \left[\sum_{m=1}^{M} ILM_B(\mathbf{r}_m, \mathbf{r}_s, \omega) \underbrace{\hat{G}_0(\mathbf{r}_k, \mathbf{r}_m, \omega)^* \hat{G}_{CR}^{\sim}(\mathbf{r}_t, \mathbf{r}_k, \omega)}_{\text{mismatched and defocused}} \right. \\
&\quad \left. + ILM_C(\mathbf{r}_t, \mathbf{r}_s, \omega) \underbrace{\hat{G}_{CR}(\mathbf{r}_k, \mathbf{r}_t, \omega)^* \hat{G}_{CR}^{\sim}(\mathbf{r}_t, \mathbf{r}_k, \omega)}_{\text{matched and refocused}} \right]
\end{aligned} \tag{11}
$$

With all the ground sections refocused, the undulation information is successfully acquired and stitched together as a complete ground surface, which updates the propagation path from receiving antennas to the target and forms a new Green's function as $\hat{G}_{CR}^{\sim}(\mathbf{r}, \mathbf{r}_k, \omega)$. With

the new inversion model, $E_R^{\sim}(\mathbf{r}_k, \omega)$ is performed by TRM imaging again to refocus the buried target beneath the estimated ground. In the second iteration, the space-time signal in the image domain is expressed as Equation (11).

Now the propagation environment for the target echo is matched. The buried target will be refocused by the second TRM procedure in both time and space domain, as shown in Fig. 3(b).

The above description can be summarized as: The first TRM procedure is to image the ground surface and acquire the information of rough surface. The second TRM procedure is to image the buried target. The usage of the ground clutters is to provide the information of rough surface, which helps a lot in the second TRM imaging process.

3. NUMERICAL SIMULATION

In this section, numerical simulation by using FDTD algorithm is used to investigate the performance of Iterative TRM imaging for BOD problem. The imaging results with conventional TRM, the method of this paper and the traditional back-projection (BP) method are compared.

The simulation setup is shown in Fig. 4. The grid is set as 3.33 grids/cm. The height expectation of ground surface is set at $y_g = 0\,\mathrm{m}$. Pulse transmitter is set at $(x_s, y_s) = (1.2\,\mathrm{m}, 0.6\,\mathrm{m})$. Receiver array has 41 elements with their position given as $(x_{rk}, y_r) = (0.6\,\mathrm{m} + k * 0.03, 0.6)\,|k \in [0, 40]$. The buried target is a metal ball with a diameter of 6 cm, and centered at $(x_t, y_t) = (1.2\,\mathrm{m}, -0.3\,\mathrm{m})$. The soil has a relative dielectric constant of $\varepsilon_r = 7$ and a conductivity of $\sigma = 12\,\mathrm{mS/m}$, which is a typical permittivity of outdoor moist soil [24]. The ground surface is generated as Gaussian random rough surface with specified correlation length [25]. The root mean square

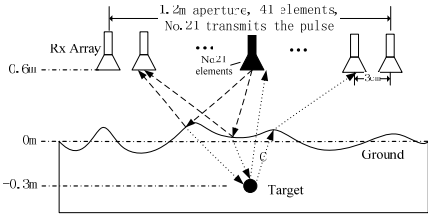

Figure 4. Setup of the simulation.

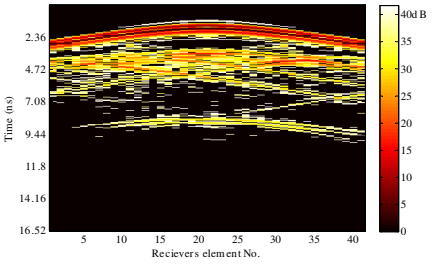

Figure 5. Signals from the linear array.

height is set to ± 9 cm, correlation length is set to insure more than 15 periods of undulation in the entire ground surface. The electromagnetic pulse is chosen as [26]

$$p(t) = \frac{j}{[j + 2\pi f(t - t_0)/4]^5}, \tag{12}$$

with a center frequency $f = 2$ GHz, band width from 1.4 GHz to 3 GHz.

The signals received by the antenna array are shown in space-time domain as in Fig. 5. The pulse is emitted by the source at time 0 ns, and direct path contributions appear around time $1.9 \sim 3.6$ ns which will be subtracted as given in Equation (1). The ground surface bouncing contributions appear around time $2.9 \sim 8.5$ ns. The target's contributions are at time-step $8 \sim 10.38$ ns. Obviously, the echo contains the contributions from the three parts as described in Section 2. In the following experiment, the iterative TRM method is applied to extract the ground surface information and image the buried target.

In the first TRM imaging procedure, the simulation environment is set as free space without soil. The goal is to focus the ground surface. The ground sections with different distances from the pulse will be refocused chronologically. The furthest section $\mathbf{r}_M$ will be firstly refocused, then $\mathbf{r}_{M-1}$, and $\mathbf{r}_1$ locating right under the pulse source at last. During the TRM procedure, when the field strength peak value appears in a small area near the expectation of ground surface, the time and the space coordinates are both recorded and considered as a successful refocusing of ground section. This focusing detection method is widely used in TRM imaging researches [18, 19]. As samples, Fig. 6 shows the refocused imaging of three ground sections located at $x = 0.6$ m, 0.9 m and 1.2 m at different time based on the space-time field peak method of focusing detection. The red line is the real ground

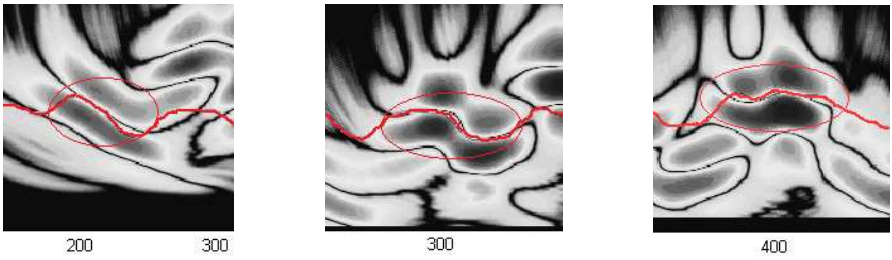

(a) time=13.3ns (b) time=13.7ns (c) time=14 ns

Figure 6. Three ground sections refocused in TRM imaging of free space.

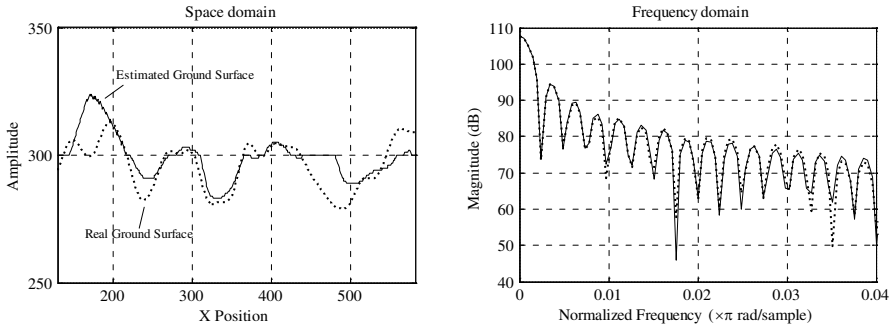

(a) (b)

Figure 7. Comparison of estimated ground with the real ground: (a) in space domain, (b) in frequency domain.

undulation. It is clear that the image of ground clutters matches the undulation quite well. By the image processing method including watersheds [27] and binarization process, the ground surface can be extracted one section after another. Then all the ground undulation is estimated and stitched together.

Figure 7 shows the space and frequency domain comparison of estimated ground with the real ground. The estimated interface matches the real interface well, especially at the center part of the ground. This is due to its relative effective larger antenna array aperture. The estimation of this part also has the most significant multi-path effects on the buried object. From Fig. 7(b), the spectrum of the estimated ground matches very well with that of the real ground.

After the first iteration of TRM imaging with the assumption of free space environment, the material beneath the updated ground surface is filled with typical moist soil [24]. Re-run the TRM imaging process, and check the time domain expression of $I_{2nd}(\mathbf{r}_t, \omega)$ given as Equation (11) to find the peak value in both space and time domain. In order to evaluate the performance of refocusing, the Imaging SNR (ISNR) is defined as [13]:

$$\mathrm{ISNR} = 20 \log \left\{ \frac{I - I_R}{I_R} \sum_{i=1}^{I_R} x_i^2 \Big/ \sum_{j=1}^{I-I_R} y_j^2 \right\} \tag{13}$$

Figure 8 shows the comparison with different methods.

Figure 8(a) is the result by using conventional TRM with exact given ground surface, where $\hat{G}_{TR}(\mathbf{r}, \mathbf{r}_k, \omega)$ is perfectly matched with $\hat{G}_{CR}(\mathbf{r}, \mathbf{r}_k, \omega)$. It is used as a reference here. The ISNR of the image is up to 35 dB. Fig. 8(b) is the result by using the assumption of a

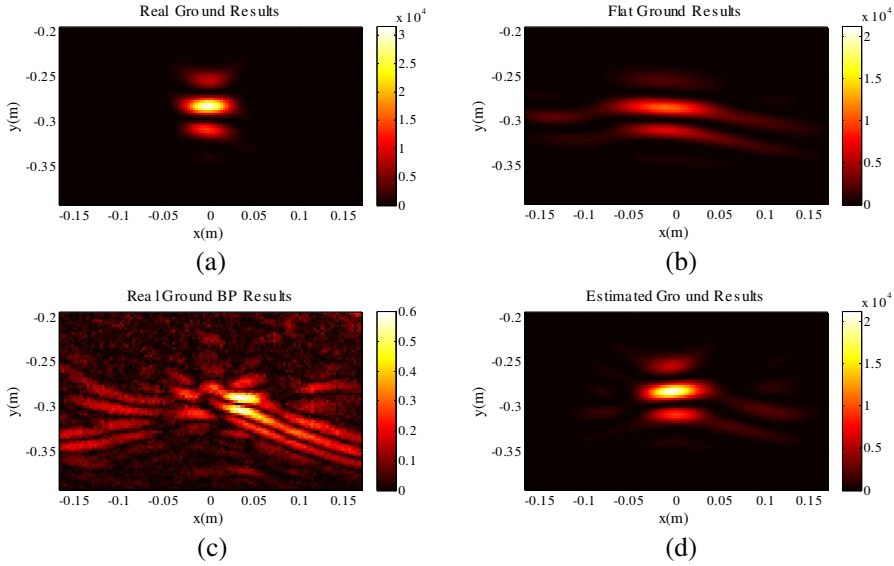

Figure 8. Imaging results comparison: (a) TRM with real ground; (b) Iterative TRM with estimated ground; (c) TRM with flat ground; (d) BP imaging with real ground.

flat ground surface in the conventional TRM. Because of the mismatch of ground surface, the ISNR is decreased to 28 dB. Fig. 8(c) is the result of tradition back projection (BP) method with the given real ground surface and gives us an ISNR of 23 dB. Comparing Fig. 8(c) with Fig. 8(b), although the conventional TRM does not use the information of ground (using flat ground instead), it still can get much better image quality than the BP method due to its consideration of the propagation progress. Fig. 8(d) is the result by using the proposed iterative TRM method, where the $\hat{G}_{TR}^{\sim}(\mathbf{r}, \mathbf{r}_k, \omega)$ is updated with the ground undulation information to match with $\hat{G}_{CR}(\mathbf{r}, \mathbf{r}_k, \omega)$. The ISNR is 32 dB. Comparing with Fig. 8(b), the ground surface information acquired from the first TRM iteration increased the image quality by $4 \sim 5$ dB.

Figure 9 shows the comparison on the target positioning accuracy and resolution. The peak position is used for the accuracy comparison and the half peak width (HPW) is used for the resolution comparison: 3.96 cm width peak centered at $x = -0.38$ cm for conventional TRM method with given real ground, 4.85 cm width peak centered at $x = -0.22$ cm for the proposed iterative TRM method, and 8.5 cm width peak centered at $x = -1.95$ cm for the conventional TRM method with the assumption of a flat ground. It is obvious that the proposed

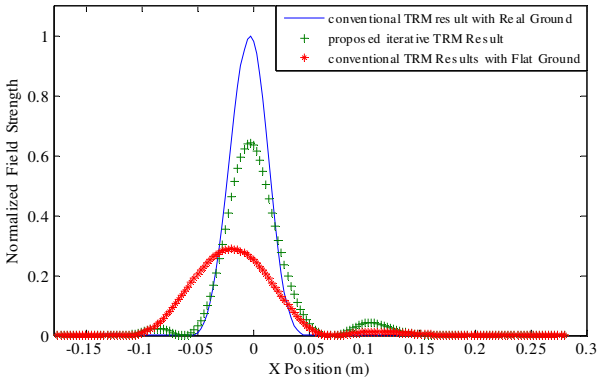

Figure 9. X-axis profile line of $y = -0.27\,\mathrm{m}$ (target position).

Iterative TRM method has almost the same positioning accuracy and resolution as the TRM method with given real ground, which means the information acquired by the first TRM procedure is correct and efficient. Without the ground surface information, the conventional TRM method leads to much worse positioning accuracy and resolution.

The advantages of Iterative TRM imaging method have been demonstrated clearly by numerical simulations. With ground surface information extracted successfully from the ground clutters, the proposed method is proved to be quite helpful to the correctness of the inversion environment and significantly improves the image quality in TRM.

4. CONCLUSION

An iterative Time-Reversal method for imaging buried target is proposed and demonstrated in this paper. Unlike the traditional signal processing methods [5–10], the information of the propagation environment is well considered here. Unlike the conventional TRM methods which based on the assumption of flat ground or exactly given ground surface [22, 23], the proposed method extracts the information of rough ground surface actively from the ground clutters. TRM operation is performed twice on the received signal. One for ground scatters in air and one for buried target in soil. The target echo is refocused and imaged finally in the estimated rough ground surface. The method is demonstrated both in theory and simulation. The numerical simulation results prove that this method performs significantly better image contrast comparing with flat ground surface model during TRM imaging. $4 \sim 5\,\mathrm{dB}$ improvement on Imaging SNR is achieved and the target is also located more precisely. The efficiency

and the spatial resolution have been improved because the information of the ground surface has been well utilized in the TRM procedure, i.e., the propagation environment has been effectively considered. However, the spatial resolution of rough ground surface also affects the imaging quality of the buried target. The quantitative analysis on this effect needs further study.

In this paper, we have chosen the BOD problem as an example to illustrate the idea of this iterative TRM method. In this example, the contributions from the environment and the target can be mostly separated. Then the information from the ground surface can be used to reconstruct the propagation environment. But in other more complicated cases, for example, a target surrounded by a cluster of complicated scatters, one may not be able to effectively extract the information of the environment. At this condition, how to use the information to rebuild the propagation environment will be more difficult. Anyway, this paper proposes the iterative idea of TRM. Using this method on some other applications such as through the wall radar and RF locating services is still an interesting problem we are working on.

ACKNOWLEDGMENT

This work is supported in part by the NSFC (No. 60927002, 60771042), China 111 Project (Grant No. B07046) and NSAF (No. 10776003).

REFERENCES

1. Pettinelli, E., A. Di Matteo, E. Mattei, L. Crocco, F. Soldovieri, J. D. Redman, and A. P. Annan, "GPR response from buried pipes: Measurement on field site and tomographic reconstructions," *IEEE Trans. Geosci. Remote Sens.*, Vol. 47, No. 8, 2639–2645, 2009.
2. Borgioli, G., L. Capineri, P. L. Falorni, S. Matucci, and C. G. Windsor, "The detection of buried pipes from time-of-flight radar data," *IEEE Trans. Geosci. Remote Sens.,* Vol. 46, No. 8, 2254–2266, 2008.
3. Daniels, D., "A review of GPR for landmine detection," *Sens. Imaging: Int. J.*, Vol. 7, No. 3, 90–123, 2006.
4. Das, Y., "Effects of soil electromagnetic properties on metal detectors," *IEEE Trans. Geosci. Remote Sens.,* Vol. 44, No. 6, 1444–1453, 2006.
5. Dogaru, T., L. Collins, and L. Carin, "Optimal time-domain detection of a deterministic target buried under a randomly rough

interface," *IEEE Trans. Antennas Propagat.,* Vol. 49, 313–326, 2001.

6. Van der Merwe, A. and I. J. Gupta, "A novel signal processing technique for clutter reduction in GPR measurements of small, shallow land mines," *IEEE Trans. Geosci. Remote Sens.*, Vol. 38, 2627–2637, 2000.
7. Runkle, P. R., P. K. Bharadwaj, L. Couchman, and L. Carin, "Hidden markov models for multi-aspects target classification," *IEEE Trans. Signal Processing,* Vol. 47, 2035–2040, 1999.
8. Sullivan, A., R. Damarla, N. Geng, Y. Dong, and L. Carin, "Ultrawide-band synthetic aperture radar for detection of unexploded ordnance: Modeling and measurements," *IEEE Trans. Antennas Propagat.,* Vol. 48, 1306–1315, 2000.
9. Dong, Y., P. R. Runkle, L. Carin, R. Damarla, A. Sullivan, M. A. Ressler, and J. Sichina, "Multi-aspect detection of surface and shallow-buried unexploded ordnance via ultra-wideband synthetic aperture radar," *IEEE Trans. Geosci. Remote Sens.*, Vol. 39, 1259–1269, 2001.
10. Cui, G., L. Kong, and J. Yang, "A back-projection algorithm to stepped-frequency synthetic aperture through-the-wall radar imaging," *Process of 1st Asian and Pacific Conference on Synthetic Aperture Radar,* 123–126, 2007.
11. Bal, G. and L. Ryzhik, "Time reversal and refocusing in random media," *SIAM Journal on Applied Mathematics*, Vol. 63, 1475–1498, 2003.
12. Zheng, W., Z. Zhao, and Z.-P. Nie, "Application of TRM in the UWB through wall radar," *Progress In Electromagnetics Research*, Vol. 87, 279–296, 2008.
13. Zheng, W.-J., Z.-Q. Zhao, Z.-P. Nie, and Q.-H. Liu, "Evaluation of TRM in the complex through wall environment," *Progress In Electromagnetics Research,* Vol. 90, 235–254, 2009.
14. Fink, M., "Time reversed acoustics," *Physics Today*, Vol. 50, 34–40, 1997.
15. Bellomo, L., S. Pioch, M. Saillard, and E. Spano, "Time reversal experiments in the microwave range: Description of the radar and results," *Progress In Electromagnetics Research*, Vol. 104, 427–448, 2010.
16. Tortel, H., G. Micolau, and M. Saillard, "Decomposition of the time reversal operator for electromagnetic scattering," *Journal of Electromagnetic Waves and Applications,* Vol. 13, No. 15, 687–719, 1999.

17. Chen, X., "Time-reversal operator for a small sphere in electromagnetic fields," *Journal of Electromagnetic Waves and Applications,* Vol. 21, No. 9, 1219–1230, 2007.
18. Liu, D., J. Krolik, and L. Carin, "Electromagnetic target detection in uncertain media: Time-reversal and minimum-variance algorithms," *IEEE Trans. Geosci. Remote Sens.*, Vol. 45, 934–944, 2007.
19. De Rosny, J., G. Lerosey, and M. Fink, "Theory of electromagnetic time-reversal mirrors," *IEEE Trans. Antennas Propagat.,* Vol. 58, 3139–3149, 2010.
20. Liu, X., B.-Z. Wang, S. Xiao, and J. H. Deng, "Performance of impulse radio UWB communications based on time reversal technique," *Progress In Electromagnetics Research*, Vol. 79, 401–413, 2008.
21. Zhang, W., A. Hoorfar, and L. Li, "Through-the-wall target localization with time reversal music method," *Progress In Electromagnetics Research*, Vol. 106, 75–89, 2010.
22. Foroozan, F. and A. Asif, "Time-reversal ground-penetrating radar: Range estimation with cramér-rao lower bounds," *IEEE Trans. Geosci. Remote Sens.*, Vol. 48, 3698–3708, 2010.
23. Bourgeois, J. M. and G. S. Smith, "A fully three-dimensional simulationof a ground-penetrating radar: FDTD theory compared with experiment," *IEEE Trans. Geosci. Remote Sens.,* Vol. 34, No. 1, 36–44, Jan. 1996.
24. Bobrov, P. P., V. L. Mironov, O. V. Kondratieva, and A. V. Repin, "Frequency dependence of permittivity of free and bound water in soils for different textures," *PIERS Online*, Vol. 5, No. 5, 426–430, 2009.
25. Tsang, L., C. H. Chan, K. Pak, and H. Sangani, "Monte Carlo simulations of large-scale problems of random rough surface scattering and applications to grazing incidence with the BMIA/canonical grid method," *IEEE Trans. Antennas Propagat.,* Vol. 43, 851–859, 1995.
26. Zhao, Z., N. Li, J. Smith, et al., "Analysis of scattering from very large three-dimensional rough surface using MLFMM and ray-based analyses," *IEEE Antennas and Propagation Magazine,* Vol. 47, 20–30, 2005.
27. Cousty, J., G. Bertrand, L. Najman, and M. Couprie, "Watershed cuts: Thinnings, shortest path forests, and topological watersheds," *IEEE Trans. Patten Analysis and Machine Intelligence,* Vol. 32, No. 5, 925–939, 2010.